Free Radical Research, February 2010; 44(2): 155–170

informa
healthcare

Verteporfin-photoinduced apoptosis in HepG2 cells mediated by reactive oxygen and nitrogen species intermediates

JENG-FONG CHIOU[1,2], YU-HUEI WANG[2], MEI-JIE JOU[3], TSAN-ZON LIU[2], & CHIA-YANG SHIAU[1]

[1]*Graduate Institute of Medical Sciences, School of Medicine, National Defense Medical Center, PO Box 90048-518, Taipei, Taiwan,* [2]*Cancer Center and Department of Radiation Oncology, Taipei Medical University and Hospital, Taipei, Taiwan, and* [3]*Department of Physiology and Pharmacology, Chang Gung University, Kwei-Shan, Taoyuan, Taiwan*

(Received 10 May 2009; revised 28 September 2009)

Abstract

Photodynamic therapy (PDT) is a rapidly evolving treatment modality with diverse usages in the field of cancer therapy. Most of PDT is based on free radical-mediated photo-killing of cancer cells. This study aimed to elucidate the detailed cascade of events that lead to apoptotic cell death of HepG2 cells resulting from the photodynamic effect (PDE) of verteporfin. PDE of verteporfin could rapidly provoke hyper-oxidative stress and caspase activity. Glutathione (GSH) depletion and lipid peroxidation phenomena could simultaneously be evoked. The membrane integrity was decreased and permeability as reflected by the depolarization of the mitochondrial membrane potential ($\Delta\psi_m$) increased, resulting in a sudden influx of cytosolic calcium into the mitochondria. Altogether, it is suggested that these events serve as the final arbitrator to initiate the lethal apoptotic process of HepG2 cells under PDE. In addition, the data are consistent with the notion that GSH depletion is an effective strategy to sensitize cancer cells to undergo apoptosis.

Keywords: *Benzoporphyrin monoacid ring A, photodynamic therapy, glutathione depletion; lipid peroxidation, mitochondrial calcium overload, free radicals, apoptosis*

Introduction

Photodynamic therapy (PDT) is a rapidly evolving modality for the treatment of neoplastic and non-neoplastic diseases. PDT relies on the availability of certain photosensitizing agents, usually porphyrins and porphyrin-related macrocycles, to absorb light and convert this energy into cytotoxic molecules for the purpose of eradicating cancer cells efficaciously. However, it has been documented that the first generation of photosensitizers exhibit cellular toxicity even without photo-irradiation, known as 'dark toxicity'. To remedy this drawback, second generation photosensitizers are being developed, which ideally possess minimal dark toxicity and to beare rapidly cleared from normal tissue. The benzoporphyrin derivative monoacid ring A (verteporfin) is such a second-generation photosensitizer that has several characteristics favourable for utilization in PDT [1]. This agent, is chemically pure, in contrast to porphyrinmaterials like photofrin, which isare a mixture, and can be activated with light of wavelength 690 nm, which is long enough to allow good theoretical penetration of light theoreticallyinto the deeper tissue layers required for therapy.

The mitochondrion, due to its pivotal role in arbitrating cell apoptosis [2–4], has been considered as a novel pharmacological target for various clinical applications including cancer therapy [5–7]. It has been documented that mitochondrial dysfunction can lead to mitochondrial membrane potential depolarization and ATP depletion, which then enhances the leakage of electrons from the respiratory chain,

Correspondence: Chia-Yang Shiau, Graduate Institute of Medical Sciences, School of Medicine, National Defense Medical Center, PO BOX 90048-518, Taipei, Taiwan. Tel/ Fax: +886-2-87924857. Email: cys@ndmctsgh.edu.tw

ISSN 1071-5762 print/ISSN 1029-2470 online
DOI: 10.3109/10715760903380458

leading to the formation of more reactive oxygen species (ROS), which will in turn damage mitochondria further. This self-perpetuating vicious cycle may play a critical role in induction of more harmful mitochondrial ROS (mROS) and singlet oxygen formation. Recently, Peng et al. [8] demonstrated that verteporfin mainly localizes in the mitochondria of intact C6 glioma cells. Following laser-irradiation at 690 nm onof C6 glioma cells, ROS productioned was mainly found concentrated in the mitochondria and apoptotic cell death was also detected afterwardsubsequently. However, the detailed cascade of events leading to the final occurrence of apoptotic cell death remain to be delineated. Thus, it will be of interest to clarify the underlying mechanism of action instigated by the photodynamic effect of verteporfin and to dissect the possible early upstream events that may lead to the final demise of the cells. Specifically, several important questions need to be addressed: (1) besides documented ROS production [9–16], can the PDE of verteporfin also generate reactive nitrogen species (RNS), such as nitric oxide (NO)?; (2) what are the early upstream events that result from mROS accumulation and can the generated mROS provoke intracellular glutathione (GSH) depletion and lipid peroxidation?; (3) can the PDE of verteporfin simultaneously elicit an alteration of calcium (Ca^{2+}) homeostasis? If yes, could this phenomenon serve as a trigger for apoptotic cell death of HepG2, a cell line highly resistant to chemotherapy and radiation ? In this study, these questions have been addressed were using a probe-based confocal imaging technique, which allows the observation of evoked phenomenon at the single cell level and in real time.

Materials and methods

Cell culture

HepG2 cell, a hepatoblastoma subline, was used for this study. All cells were grown in medium consisting of Dulbecco's modified Eagle's medium (Life Technologies, Grand Island, NY) supplemented with 10% (v/v) foetal bovine serum (FBS), at 37°C in a CO_2 humidified incubator. The cells were plated onto glass coverslips coated with poly-L-lysine for fluorescent measurement (Model No. 1, VWR Scientific, San Francisco, CA).

Chemicals and fluorescent dyes

Verteporfin was provided by Quadra Logic Technologies Inc. (Vancouver, BC, Canada). Verteporfin was protected from light and maintained at 4°C until use. All fluorescent dyes were purchased from Molecular Probes Inc. (Eugene, OR) and chemicals were obtained from Sigma (St. Louis, MO). Loading concentrations of fluorescent probes were as follows: mitochondrial fluorescent dye: Mitotracker green (Mito G) 100 nM; ROS fluorescent dye: 6-carboxy-2',7'-dichlorodihydrofluorescein diacetate (DCF-DA) [17,18], 500 nM; calcium mobilization detective dyes: RHOD-2/AM (rhod-2) 1.5 μM and FLUO-4/AM (fluo-4) 2 μM. Lipid peroxidation detecting probe: C_{11}-BODIPY $^{581/591}$ [19], 10 mM; GSH depletion detection probe: chloromethyl fluorescein diacetate (CMF-DA) [20], 25 μM; mitochondrial membrane potential dye: tetramethylrhodamine methyl ester (TMRM), 500 nM and the ratiometric indicator 5,5',6,6'-tetrachloro-1,1',3,3'-tetraethylbenzimidazolylcarbocyanine iodide (JC-1), 1 μM; fluorescent probes were all loaded at room temperature for 20–30 min. After loading, cells were rinsed three times with HEPES-buffered saline (140 mM NaCl, 5 mM KCl, 1 mM $MgCl_2$, 2 mM $CaCl_2$, 10 mM glucose, 5 mM HEPES, pH 7.4). Cells loaded with DCF-DA required an additional 30–40 min of incubation after the dye loading to allow intracellular deacetylation of the ester form of the dye. All experiments were performed in HEPES-buffered saline.

Photosensitization protocol of verteporfin in HepG2 cell

For the photosensitization experiments, a stock solution of verteporfin at 1 mg/mL in phosphate buffer saline (PBS) was prepared and stored at 4°C until use. Cells were incubated with verteporfin at 0.5 μg/mL or 5 μg/mL in HEPES for 30 min at 37°C and then exposed to a Coherent 690 nm diode laser with laser power of 15 mW. Laser irradiation strength of 5 J (5 min and 30 s) was applied. To investigate the cellular distribution of verteporfin, cells were treated with 5 μg/ml verteporfin. To allocateconfirm its location in the mitochondrion, verteporfin and Mito G were co-loaded for incubation with cells. Confocal images of verteporfin and Mito-G were collected simultaneously.

Confocal imaging microscopy

Confocal fluorescence images were obtained using a Leica SP2 MP (Leica-Microsystems; Mannheim, Germany) fibre coupling system equipped with a Ti:Sa-Laser system equipped with an Ar/Kr laser and filters specific for FITC (Exi: 488 nm; Emi: 530/30 nm) and TRITC (Exi: 543 nm, Emi: 590 nm) (model: Millenia/Tsunami; Spectra-Physics; Mountain View, CA) providing pulse repetition rate at 82 MHz, laser pulse width of 1.2 ps, spectral bandwidth of 1 nm and object pulse width of 1.3 ps). A wavelength of 800 nm with an average laser power of 600 mW was selected for illumination. The size of the pinhole was set at 5% open to provide confocal imaging and less marked photo bleaching

effects. During fluorescence imaging, the illumination light was reduced to a minimal level by selecting suitable neutral density filters (3%) according to the real situation of different probes in control experiments to prevent the photosensitizing effect from the interaction of light with fluorescent probes. All images were processed and analysed using Leica QWin software (Leica Imaging Systems Ltd., Cambridge, UK). Intensity levels were analysed from the original images and graphed by using SigmaPlot and Image J software.

Flow cytometry

A Becton-Dickinson FACS-Calibur flow cytometer was used; 10^4 cells were recorded and fluorescence intensities were measured on a logarithmic scale. The flow data were analysed by CellQuest software.

Fluorescence detection of intracellular ROS and RNS with confocal microscopy

Intracellular ROS was detected using DCF-DA which has been reported to be less sensitive to light and have better cell retention as compared to classic ROS probes such as dichlorofluorescein, upon fluorescent measurement. The non-fluorescent DCF-DA is oxidized by intracellular ROS to form the highly fluorescent DCF. Fluorescent images of DCF were obtained without or solely with 690 nm laser irradiation or under treatment with verteporfin alone or with both verteporfin and laser irradiation. To measure the production of intracellular NO, cells were cultured in poly-L-lysine coated slides in 3-cm culture dishes. After reaching 80% cell density, cells were incubated with 2 μM DAF-FM diacetate in HEPES for 30 min in the dark. The cells were then mounted on the stage of a Leica SP2 laser scanning confocal microscope. The cells were randomly selected and imaged. Pre-treatment with N-acetyl cysteine (NAC) at 20 μM for 2-h was carried out when required.

Measurement of mitochondrial membrane potential ($\Delta\psi_m$)

$\Delta\psi_m$ was measured with the fluorescent lipophilic cationic dye tetramethylrhodamine methyl ester (TMRM, 500 nM) and the ratiometric indicator 5,5',6,6'-tetrachloro-1,1',3,3'-tetraethylbenzimidazolylcarbocyanine iodide (JC-1, 1 μM) that accumulates within mitochondria, depending on the $\Delta\psi_m$. Before the PDT of verteporfin, cells were stained with TMRM or JC-1 for 15 min and ~ 100 cells were randomly selected for fluorescence confocal imaging. Pre-treatment with N-acetyl cysteine (NAC) at 20 μM for 2-h was carried out when required.

Fluorescence detection of lipid peroxidation with confocal microscopy

C_{11}-BODIPY$^{581/591}$, a lipophilic fluorescent probe, was measured to estimate the extent of lipid peroxidation occurring during the PDE of verteporfin. Peroxidation of C_{11}-BODIPY$^{581/591}$ was accompanied by a shift in fluorescence from red to green and the relative value of non-oxidized probe was analysed and presented as the ratio of red:(red + green) fluorescence as detected by using confocal microscopy. The cells were loaded with 10 mM C_{11}-BODIPY$^{581/591}$ in dimethyl sulphoxide (DMSO; final concentration 0.1%) for 30 min at 37°C in the dark. Red and green fluorescence were determined and analysed by a Leica SP2 MP confocal imaging microscopy system.

Imaging and quantification of GSH content in subcellular compartments

Chloromethyl-fluorescein-diacetate (CMF-DA), containing a mild thiol reactive chloromethyl reactive group, is colourless and non-fluorescent. This probe is primarily conjugated to the abundant tripeptide glutathione by glutathione S-transferase. Once inside the cell, cytosolic esterases cleave off the acetate groups and then the chloromethyl group reacts with intracellular thiols, transforming the probe into a cell-impermeant fluorescent dye-thioether adduct. In this experiment, cells were loaded with 25 μM CMF-DA for 30 min at 37°°C to measure the level of intracellular GSH before and after the PDE of verteporfin by a Leica SP2 MP confocal imaging microscopy system. In CMF images, GSH was calculated from areas based on a MTR distribution from the same cell. Intensity values were analysed per pixel from the cytosolic, the mitochondrial and the nuclear area of the cells by Leica QWin software.

Fluorescence detection of mitochondrial and cytosol calcium with confocal microscopy

HepG2 cells were dually stained with 1.5 μM rhod-2 and 2 μM fluo-4 to detect mitochondrial and cytosolic calcium, respectively. Fluorescent images of rhod-2 and fluo-4 were obtained before and after the treatment with only 690 nm laser irradiation, verteporfin alone or the combination of both verteporfin and laser-irradiation.

MTT assay

HepG2 cells were plated at 3×10^5 per well in a 6-well plate and incubated for 2 days at 37°C in a humidified incubator containing 5% CO_2. When the viability of HepG2 cells under PDE of verteporfin were measured, 1 ml of 0.5 mg/ml MTT salt per well was added to and incubated for 3 h. Afterwards, the

supernatant of each well was discarded and 0.5 ml DMSO added and then further incubated for another 30 min. Absorbance can be read at 550 nm in a Beckman DU-640 spectrophotometer. The viability was calculated as percentage of that of HepG2 cells without PDE; 1 mM of EGTA was added when PDE of verteporfin was carried out in the absence of calcium.

Visualization of cytochrome **c** *release*

After PDE of verteporfin, HepG2 cells were fixed with 4% paraformadehyde at the indicated time point. Cytochrome *c* was detected by using SelectFX Alexa Fluor 488 Cytochrome *c* Apoptosis Detection Kit (Invetrogen, Molecular Probes, CA) according to the manufacturer's instructions. The distribution of cytochrome *c* was recorded and analysed using a Leica SP2 MP confocal microscopy system.

Measurement of caspase 3/7 activity

The activity of caspase 3/7 was detected before and after the photosensitization protocol by using the Apo-ONE Homogeneous Caspase-3/7 assays kit according to the manufacturer's instructions (Promega Corporation, Madison, WI). The fluorescence intensity representing the level of activated caspase 3/7 was determined at a maximum emission 521 nm in a Molecular Devise SPETRA MAX GEMINE XS fluometer.

Apoptotic DNA ladders and TUNEL assay

Apoptotic DNA ladders were analysed using the ApoAlter LM-PCR^{TM} Ladder Assay Kit from Clontech (Palo Alto, CA), which specifically amplify nucleosomal ladders generated during apoptosis. Briefly, cellular DNA was extracted and treated with RNase A and Proteinase K. The LM-PCR assay was performed according to the user manual (15 PCR cycles); 15 µl of each PCR product was electrophoresed on a 1.2% agarose/EtBr gel at 6 V/cm for ~ 2.5 h and DNA was detected by ethidium bromide under UV light. Apoptotic cell death was also confirmed by using an Apo-BrdU *in situ* DNA Fragmentation Assay Kit (BioVision, Mountain View, CA). In TUNEL assay (terminal dUTP nick-end labelling), the terminal deoxynucleotidyl transferase (TdT) in assay *in situ* transfers BrdUTP to the free 3'-OH of cleaved DNA of apoptotic cells. The BrdU-labelled cleavage sites were then visualized by reaction with fluorescein-conjugated anti-BrdU monoclonal antibody. After the incubation period, cells were washed twice with PBS, fixed for 1 min with ice-cold ethanol/acetic acid (1:1) solution and then washed three times with PBS. The fixed cells were permeabilized in ice-cold 0.2% Triton X-100 detergent for 5 min and then washed three times with PBS. Finally, the photomicrographs were obtained with Leica SP2 MP confocal microscopy.

Statistical analysis

Data were presented as mean and standard deviations from at least three independent experiments and analysed using student's *t*-test. A *p*-value of less than 0.05 was considered as statistically significant.

Results

Verteporfin is a mitochondrially-directed photosensitizer that rapidly generates ROS and RNS was lyed

Prior to testing the PDE of verteporfin on HepG2 cells, we first evaluated the localization of this photosensitizer using Mitotracker Green (Mito G). As evident from Figure 1, the fluorescence of verteporfin (red) and Mito G (green) were found to superimpose to a significant extent quite much (Figure 1) , attesting that verteporfin is a mitochondrially-directed photosensitizer. Next, we set out to clarify whether or not the probes used for detection of ROS (DCF-DA) and RNS (DAF-DA) in our studies could produce background fluorescence. In this regard, we

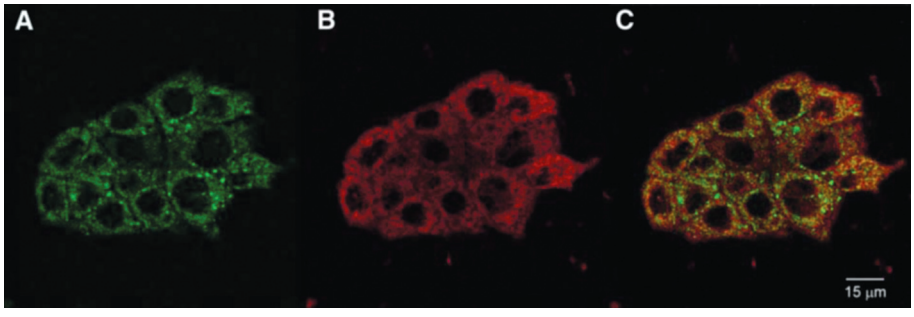

Figure 1. Evidence that verteporfin is a mitochondrion-directed photosensitizer. HepG2 cells were co-incubated with Mitotracker Green and verteporfin. It was shown that both fluorescence co-localized at mitochondria. (A) Fluorescence image of Mitotracker Green (green fluorescence). (B) Fluorescence image of verteporfin (red fluorescence). (C) Merged image of the green and red fluorescence which clearly demonstrates that verteporfin is a mitochondrion-targeted photosensitizer.

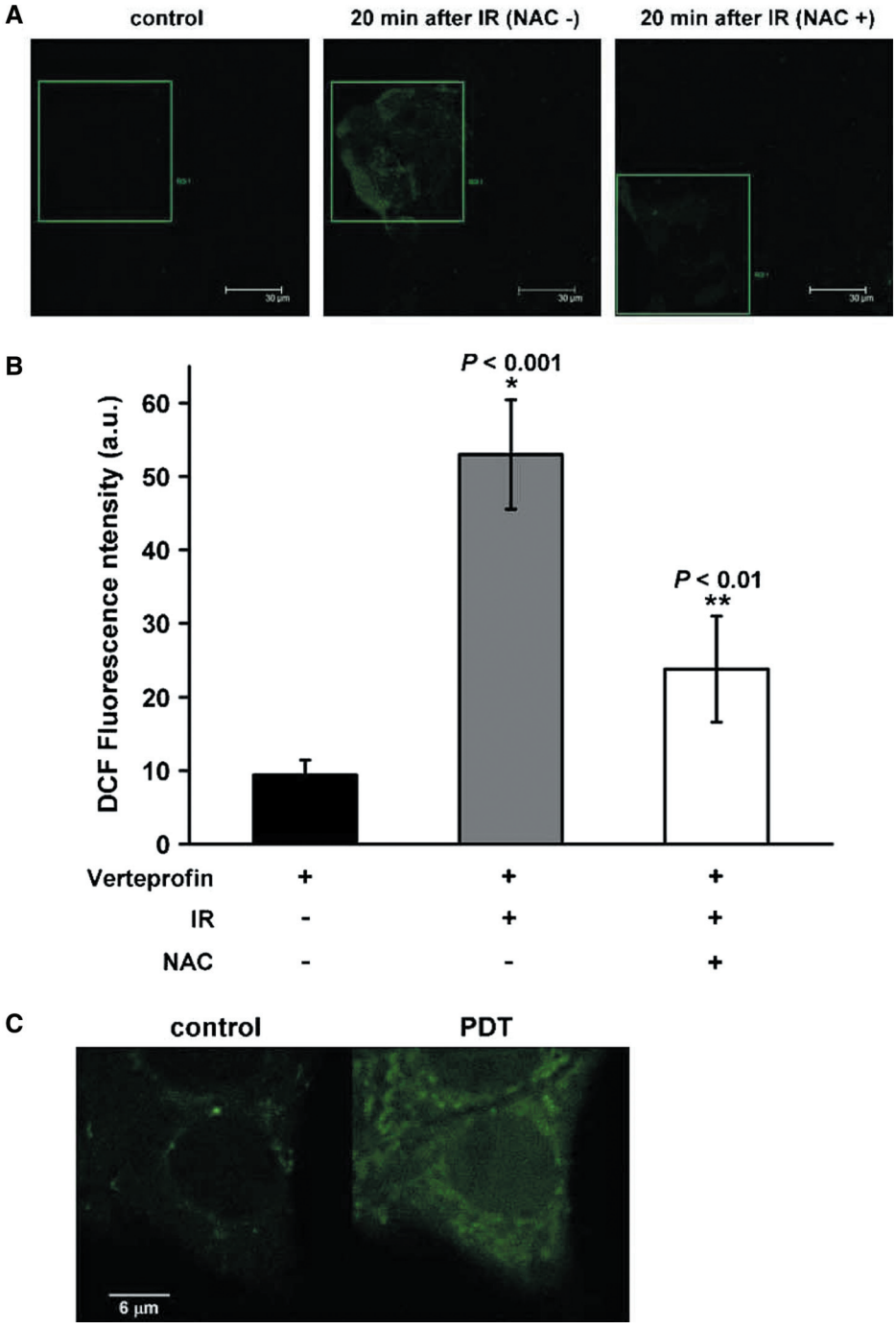

Figure 2. Verteporfin coupled with laser irradiation (690 nm) enhanced mROS formation in HepG2 cells. (A) Cells were stained with DCF (1 μM) in the dark and subjected to irradiation with or without pretreatment of NAC at 20 μM for 2-h. Note that irradiation was selectively performed only in the confined green box area as indicated. (B) The fluorescence intensities were quantified and represented using bar graphs. Prior to laser irradiation, the auto-oxidation of DCF probe within the green box area was minimal indicating that the background fluorescence of the probe was too low to be able to be detected by DCF probe. (C) The magnified image. IR, irradiation.

performed photoirradiation experiments in a selected area confined by a green box (Figures 2A and 3A).

As shown in Figure 2A (left), when HepG2 cells were treated with verteporfin and stained with DCF-DA without laser photoirradiation, the green fluorescence of DCF, an indication of probe being oxidized by ROS, was essentially minimal. This result indicates that DCF-treated cells generated insignificant background fluorescence in the absence of photoirradiation. However, when the same selected area received photoirradiation, we observed a obviousmarked increase in green DCF fluorescence. This phenomenon indicates that a significant amount of ROS was generated following photoirradiation. Without verteporfin, photoirradiation itself did not induce ROS (data not shown). Interestingly, when these cells were pre-treated with NAC, a known ROS scavenger, we found that a significant amount of the DCF fluorescence could be suppressed

(Figure 2B). These data further confirm the notion that the DCF fluorescence detected after PDE of verteporfin is truly derived from ROS oxidized DCF. It is worth noting that the DCF fluorescence generated after PDE of verteporfin was found to be confined around the perinuclear region superimposing the localization of mitochondria (Figure 2C). This, along with the mitochondrially-directed nature of verteporfin, provides evidence that ROS produced following PDE of verteporfin indeed arose mainly from mitochondria (referred to as mROS). The detection of nitric oxide (NO) generated after PDE of verteporfin on HepG2 cells was performed in an analogous manner to the experimental protocol used for ROS measurement. HepG2 cells were stained with a non-fluorescent DAF-DA probe (5 μM) in the dark and subject to photoirradiation in the presence of verteporfin (5 μg/ml) in a selected area confined by the green box. Prior to receiving photoirradiation, it was shown that verteporfin-treated HepG2 cells exhibited only a minimal amount of DAF fluorescence, as seen in Figure 3A (left).

However, immediately after these cells received photoirradiation, a markedly increased amount of DAF fluorescence (oxidation of DAF probe by NO) could be detected. Without verteporfin, photoirradiation itself did not induce NO (data not shown). However, pre-treatment of verteporfin-incubated HepG2 with NAC (20 μM), an effective NO scavenger, resulted in a nearly complete suppression of green fluorescence arising from the DAF probe. These data demonstrate that PDE of verteporfin could also generate RNS, which localized mainly in the perinuclear area, resembling the localization of mitochondria (Figure 3C).

PDE of verteporfin on Hep G2 cells can provoke intracellular GSH depletion

GSH is not synthesized in the mitochondria and must be synthesized in the cytosol and transported into mitochondria by a specific transporter. It was therefore anticipated that GSH reserves in the mitochondria might be limited. Consequently, GSH levels in the mitochondria might be rapidly depleted when excessive mROS/mRNS production surpassed the GSH-mediated antioxidative capacity of this organelle.

As revealed in Figure 4A, the PDE of verteporfin could indeed trigger time- and dose-dependent GSH depletion, as reflected by the rapid loss of CMF-GSH derived green fluorescence. Notably, more than 90% of mitochondrial GSH (mGSH) was found to be depleted 10 min after HepG2 cells were exposed to the PDE of verteporfin. This GSH depletion arising from the PDE of verteporfin was confirmed by flow cytometric analysis (Figure 4B).

The PDE of verteporfin on Hep G2 cells can induce lipid peroxidation

Phospholipid components of cellular membranes are a highly vulnerable target due to the susceptibility of its polyunsaturated fatty acid side-chains to free radical attack. Therefore, it was of interest to explore if PDE of verteporfin can also elicit lipid peroxidation in HepG2 cells. For this study, we utilized 4,4-difluoro-5-(4-phenyl-1,3-butadienyl)-4-bora-3a,4a-diaza-s-indacene-3-undecanoic acid (C_{11}-BODIPY $^{581/591}$) as a probe [19,20]. Peroxidation of this probe was accompanied by a shift in fluorescence from red to green. The ratio of red:(red + green) fluorescence as detected by the confocal microscopic imaging was presented to reflect the non-oxidized probe remaining. Our data indicates that PDE of verteporfin could also evoke lipid peroxidation of HepG2 cells in a time- and dose-dependent fashion (Figure 4C). Flow cytometric results also correlated concordantly with the results obtained by the confocal imaging method (Figure 4C (c-3)).

PDE of verteporfin on the mitochondrial function

Mitochondrial function was studied by imaging mitochondrial morphology, mitochondrial membrane potential variation and the opening of the mitochondrial permeability transition pore (MPTP). Mitochondrial membrane potential ($\Delta\psi_m$) was detected using either JC-1 or tetramethyl rhodamine ethyl ester (TMRM) (Figure 5).

JC-1 measured both high (J-aggregated red fluorescence) and low (monomer green fluorescence) mitochondrial membrane potential. As indicated in Figure 5A, confocal JC-1 imaging demonstrated that $\Delta\psi_m$ in control HepG2 cells was heterogeneous. Both high (red fluorescence) and low (green fluorescence) mitochondrial membrane potentials were detected (Figure 5A (a-1 and a-2)). Soon after PDE of verteporfin, a large and abrupt depolarization of $\Delta\psi_m$ was noted, as reflected by an instantaneous and nearly complete loss of both high and low mitochondrial membrane potentials (Figure 5A (a-3 and a-4)). In addition, we also confirmed the occurrence of $\Delta\psi_m$ changes induced by the PDE of verteporfin by using the TMRM probe. As indicated in Figure 5B, time-lapse tracing of TMRM fluorescence intensities revealed that the initial ascending phase represented the quenching effect of TMRM fluorescence after photoirradiation was initiated. As the depolarization of $\Delta\psi_m$ continued, TMRM completely detached from the mitochondrial membrane and diffused away as reflected byand subsequently a time-dependent descending phase was observed. This was a true reflection of the depolarization of mitochondrion (Figure 5B).

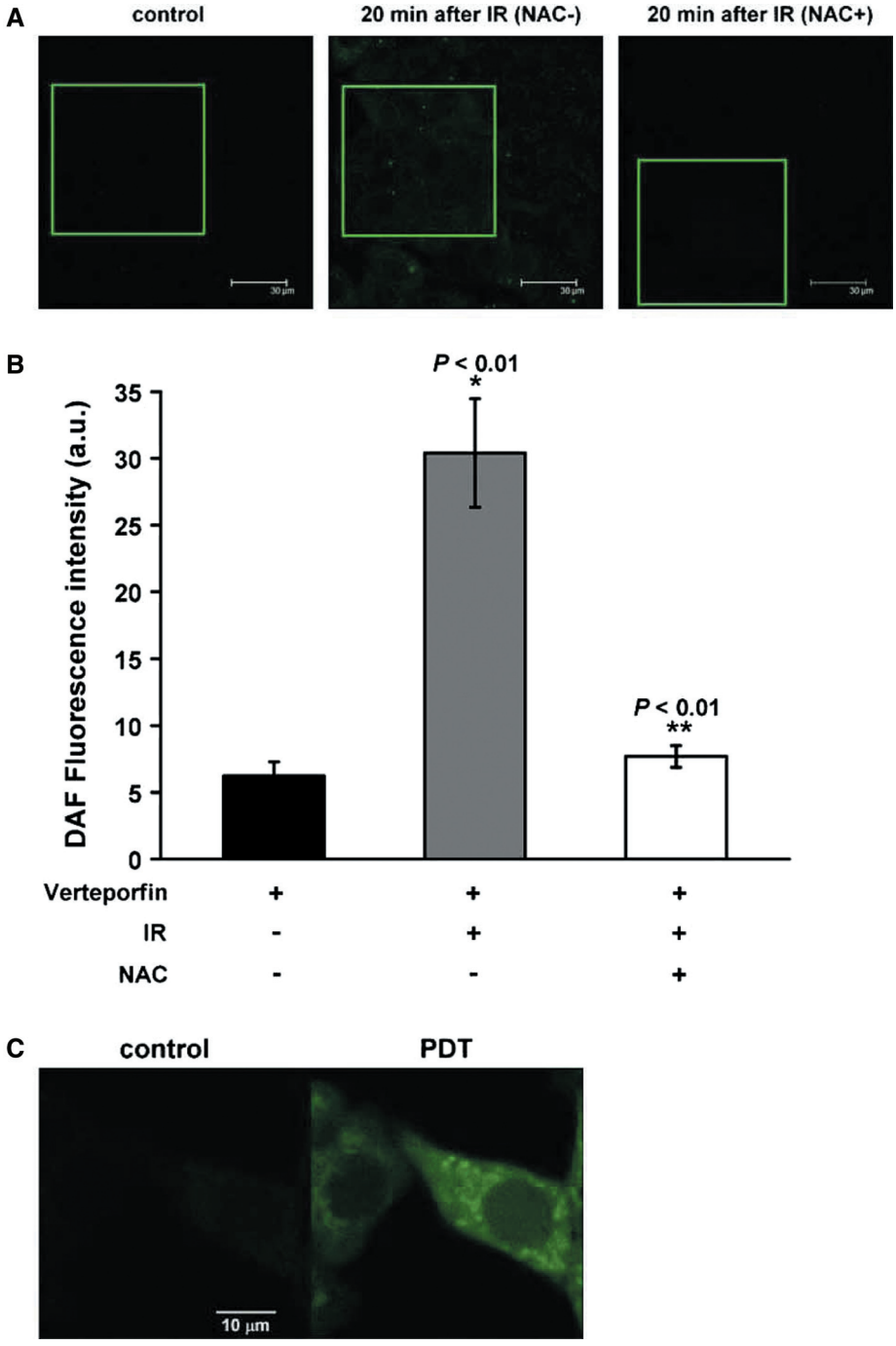

Figure 3. Verteporfin coupled with laser irradiation (690 nm) generated nitric oxide (NO) in HepG2 cells. (A) Cells were stained with DAF (5 μM) in the dark and subjected to irradiation with or without pretreatment of NAC at 20 μM for 2-h. Note that irradiation was selectively performed only in the confined green box area as indicated. (B) The fluorescence intensities were quantified and represented using bar graphs. Prior to irradiation, the auto-oxidation of DAF probe within the green box area was minimal, indicating that the background fluorescence of the probe was too low to be detected by DAF. (C) The magnified image.

PDE of verteporfin on the calcium homeostasis of HepG2 cells

We utilized a double probe approach for localizing Ca^{2+} in various compartments of the model cells, namely: fluo-4 for cytosolic Ca^{2+} (cCa^{2+}) and the acetyl methyl ester form of rhodamine-based indicator (rhod-2-AM) for mitochondrial Ca^{2+} (mCa^{2+}). The latter probe is a cationic compound, which preferentially accumulates in mitochondria through a potential-driven uptake. In the resting condition, the rhod-2 probe was incapable of eliciting fluorescence because the mCa^{2+} concentrations were too low (100–150 nM). Conversely, if a drastic influx of excessive cCa^{2+} into mitochondria surpassed a threshold concentration (~ μM range), the fluorescence of rhod-2 probe would be strongly emitted in a dose-dependent manner.

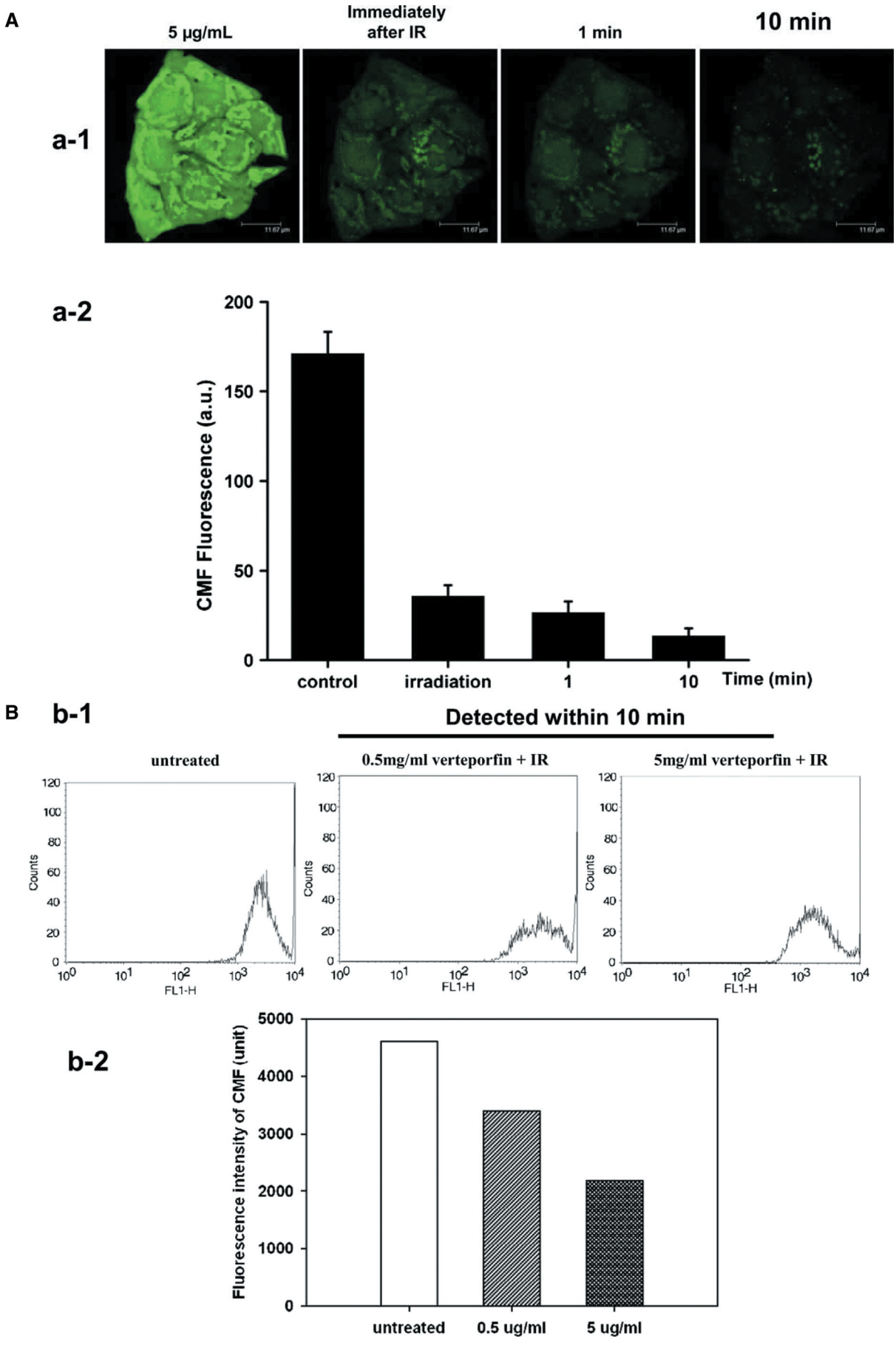

Figure 4. *(Continued)*.

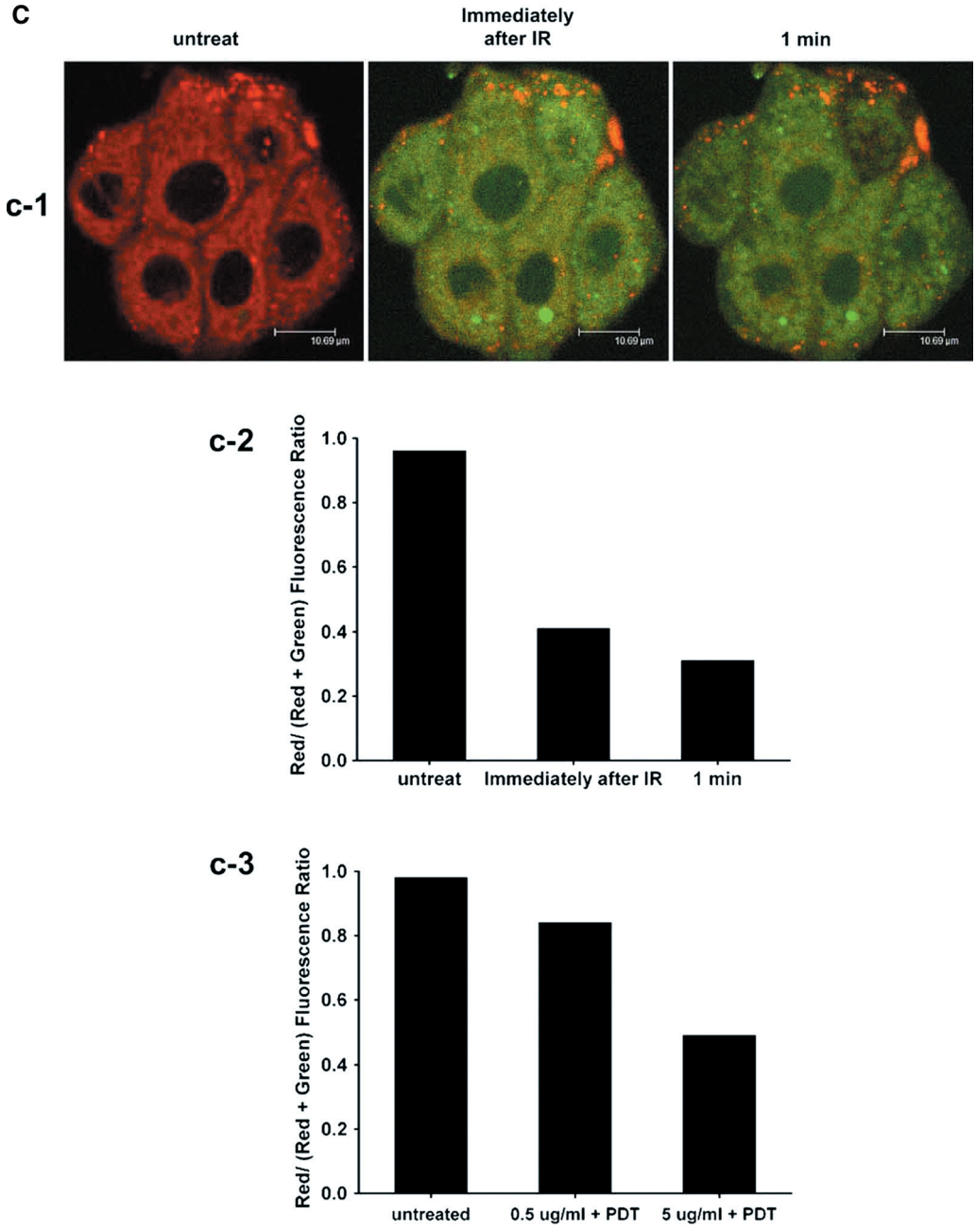

Figure 4. The PDE of verteporfin-induced intracellular GSH depletion and lipid peroxidation in Hep G2 cells. (A) Cells were stained with CMF-DA (25 μM) in the dark and subjected to irradiation in the presence of verteporfin (5 μg/ml). a-1, confocal images immediated after irradiation, 1 and 10 min. Bar = 10 μm, a-2, fluorescent level of a-1 graphed using SigmaPlot and Image J software, (B). The GSH depletion was further confirmed by a flow cytometric system (b-1) and the degree of discrepancy was assessed by bar graphs as indicated in b-2. (C) The PDE of verteporfin induced lipid peroxidation of HepG2 cells was detected by using a lipophilic fluorescence probe, C_{11}-BODIPY (c-1), the degrees of peroxidation were assessed by bar graphs as indicated in c-2. This lipid peroxidation phenomenon was further confirmed by a flow cytometric system, as indicated in c-3.

As indicated in Figure 6A, PDE of verteporfin not only triggered an increase of cCa^{2+} mobilization, but was also capable of evoking mCa^{2+} overload as a result of a sudden influx. The fluorescence intensity of rhod-2 primarily appeared in the perinuclear region, consistent with mitochondrial localization. In addition, magnified confocal images revealed that the PDE of verteporfin could also cause an alteration of mitochondrial morphology, as evidenced by a shift from an elongated thread-like shape to an oval-like contour, indicating the presence of markedly swollen mitochondria (Figure 6B).

MTT viability assay of HepG2 under PDE

As seen in FfFigure 6C, the cell viability of HepG2 cells exposed to PDE was diminished markedly. Without photoirradiation, verteporfin did not affect

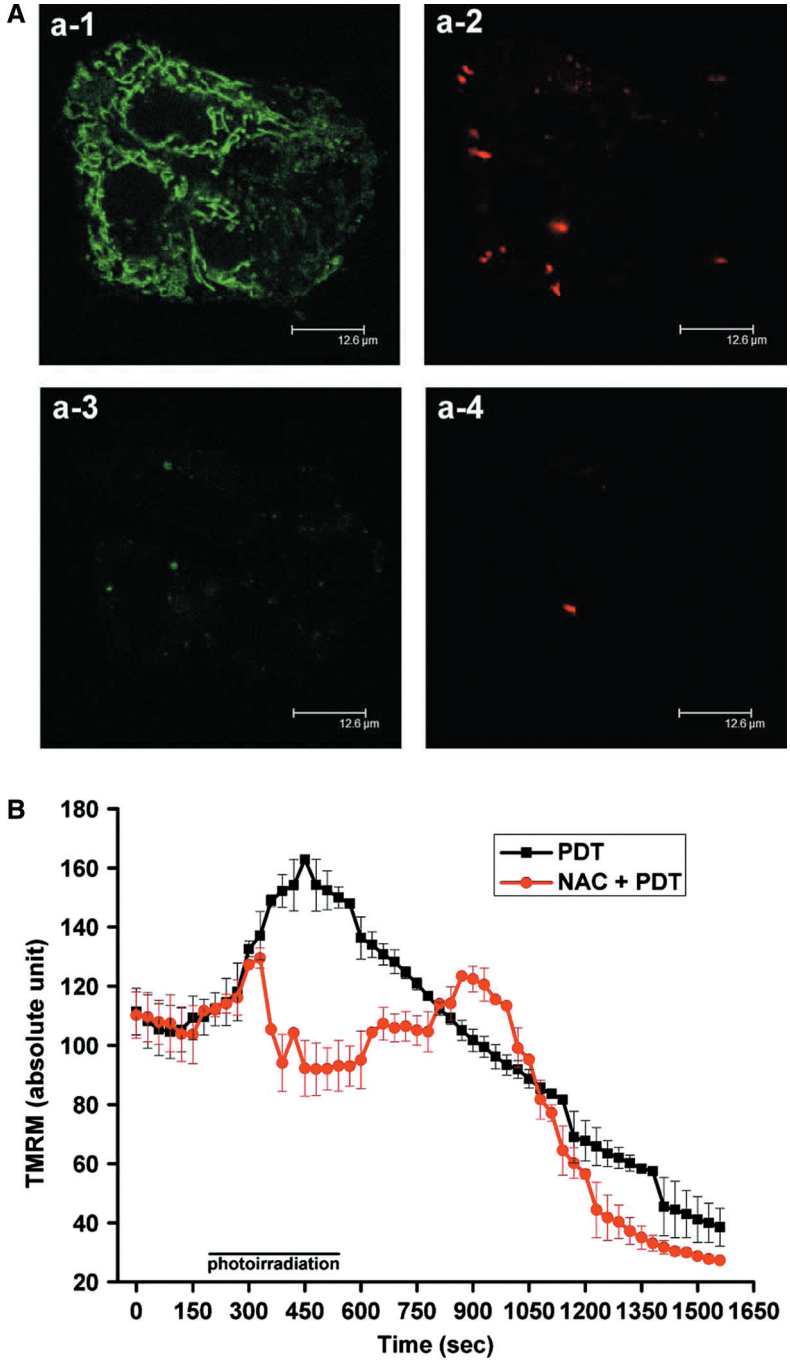

Figure 5. Measurement of mitochondrial membrane potential during the PDE of verteporfin on Hep G2 cells by the confocal imaging system. (A) JC-1 measured both high (J-aggregate red fluorescence) and low (monomer green fluorescence) mitochondrial membrane potential. Prior to PDE of verteporfin (a-1 and a-2), soon after photoirradiation (a-3 and a-4). (B) Cells were stained with TMRM (500 nM) in the dark and subjected to irradiation without or with pre-treatment of NAC at 20 μM for 2-h (> 100 cells were counted and analysed).

HepG2 cell viability too much in contrast to that of PDE of verteporfin. Deprivation of medium calcium by using EGTA at 1 mM dramatically reduced the mitochondrial content of calcium (data not shown). However, PDE of verteporfin could still exert a marked toxic effect on HepG2 cells, even with diminished mitochondrial calcium content.

PDE of verteporfin can induce apoptotic cell death of HepG2 cells

It was shown that cytochrome *c* was released into cytosol after PDE since the green fluorescent of cytochrome *c* did not co-localize with Mito G (Figure7A). The aboveThis release of cytochrome *c* was not affected in the presence of cyclosporine at

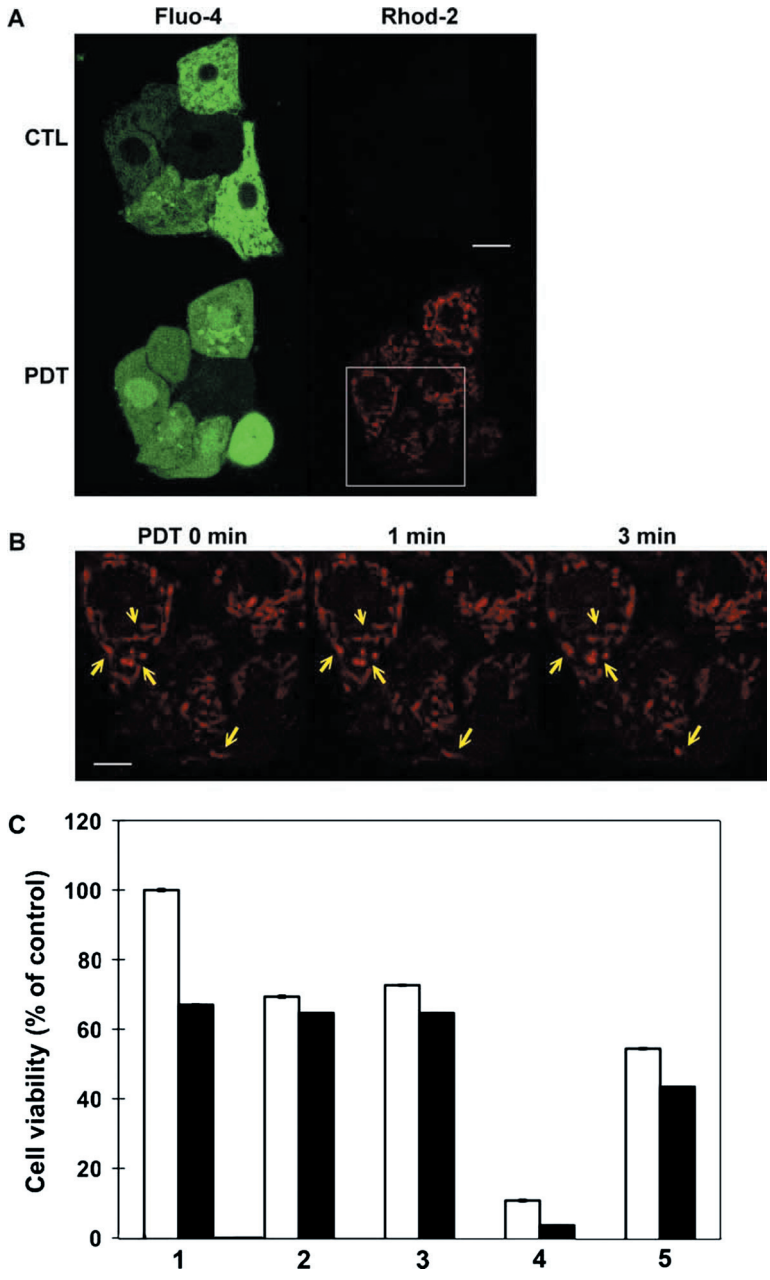

Figure 6. Imaging on cellular calcium and its involvement of cell viability under PDE of verteporfin. (A) Both cytosolic (Fluo-4 as probe) and mitochondrial Ca^{2+} (Rhod-2 as probe) were stained. White bar is 10 μm. (B) A time-lapse confocal image of Rhod-2 fluorescence after the cells received PDE of verteporfin (5 J of 690 nm for 5 min and 30 s laser irradiation), showing that mitochondria were markedly swollen resulting from a sudden influx of cytosolic Ca^{2+} into the mitochondria (yellow arrow). White bar is 2.5 μm. (C) Cell viability assay using MTT in HEPES under PDE of verteporfin of none, 5 μg/ml, 0.5 μg/ml, 5 μg/ml plus irradiation, 0.5 μg/ml plus irradiation for lane 1, 2, 3, 4, 5, respectively (white bar chart); 1 mM EGTA was added in medium when PDE was executed under deprivation of cellular calcium (black bar chart).

10 μM. Thus, release of cytochrome *c* under PDE of verteporfin was independent of mPTP opening. Also, caspase activity was rapidly raisincreased underas a result of PDE and diminished in the presence of the pancaspase inhibitor zVAD-fmk at 50 and 100 μM (Figure 7B). To verify further that cell death caused by PDE of verteporfin was apoptotic in nature, we utilized the TUNEL assay (Figure 8A). It was seen that most of HepG2 cells stained positivegreen and the stain co-localized with the nucleus, which was stained with propidium iodideethedium bromide. Furthermore, the DNA extracted from HepG2 cells was also shown tof be fragmented, as indicated by a ladder pattern on agarose gels (Figure 87B). heof cytochrome cAltogether, the data obtained unequivocally demonstrated an apoptotic nature of HepG2 cell death evoked by PDE of verteporfin.

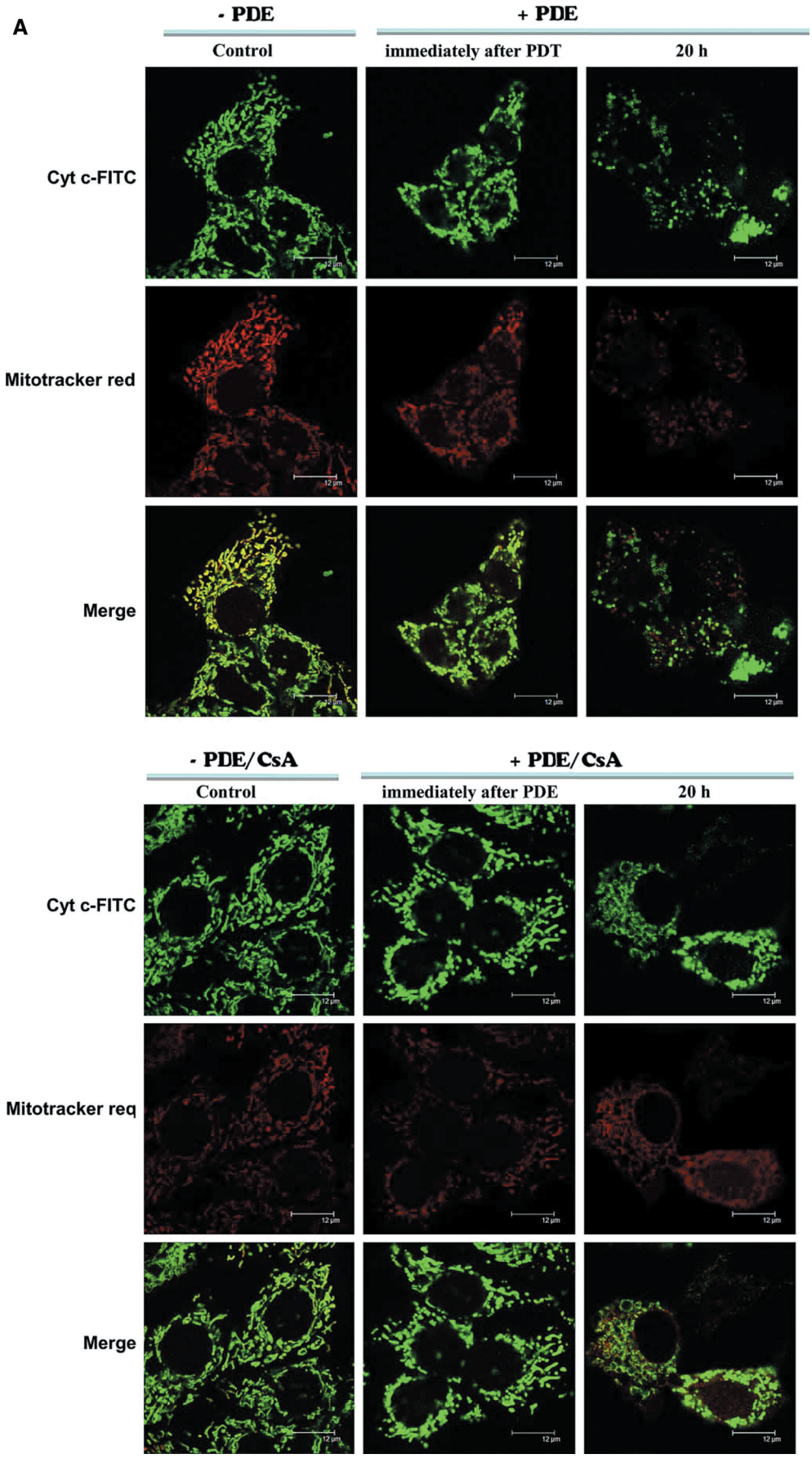

Figure 7. *(Continued)*.

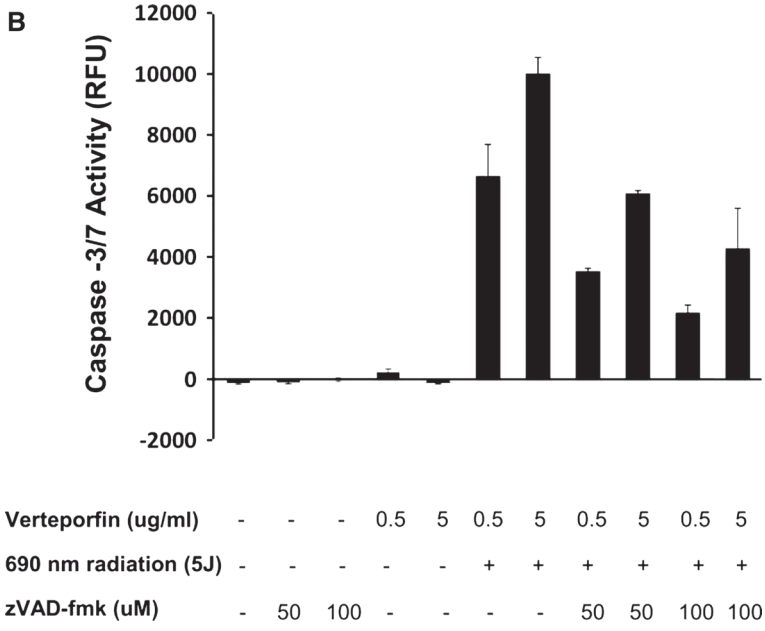

Figure 7. Imaging of cytochrome *c* and measurement of caspase activity of HepG2 under PDE. (A) Green fluorescence derived from anti-cytochrome *c* antibody conjugated with FITC with or without treatment with cyclosporine A (10 μM). (B) The caspase 3/7 activity of HepG2 under PDE was estimated with or without a pancaspase inhibitor (zVAD-fmk).

Discussion

Despite the participation of various ROS/ RNS in the mediation of PDE-induced photo-killing effects being well documented [11,12,21–24], the downstream cascade of events after the initiation of free radical production, which may be critical for the final arbitration of the lethal apoptotic cell death, has thus far been poorly elucidated. To examine this process, we selected verteporfin as a photosensitizer and HepG2 cells, a well-characterized drug- and radio-resistant HCC subline, as our experimental cell model [25]. The real time confocal imaging assay demonstrated that exposure of HepG2 cells to both verteporfin and laser irradiation at 690 nm together rapidly provoked the generation of ROS and NO, which were mainly concentrated in the mitochondria (Figures 2 and 3). These results were somewhat anticipated because we verified through the use of Mitotracker Green that verteporfin was in fact a mitochondrially-directed photosensitizer (Figure 1).

Mitochondria, due to their pivotal role in arbitrating cell apoptosis, have recently been considered as a novel pharmacological target for various clinical applications including cancer therapy [3,5–7]. In addition,

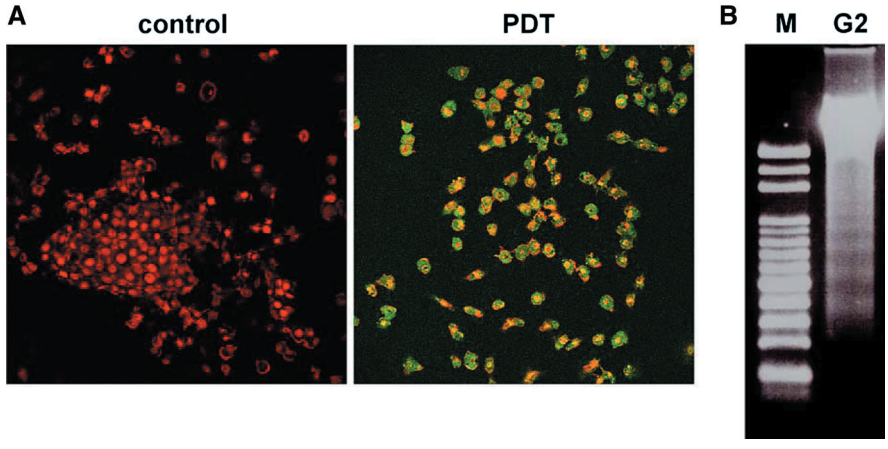

Figure 8. TUNEL assay and DNA ladder assay. (A) HepG2 cells were incubated in the medium containing 5 μg/ml of verteporfin for 30 min in the dark and subjected to photoirradiation with coherent 690 nm diode laser using strength of 5 J. TUNEL positive cells were represented here by green fluorescence and the red fluorescence of propidium iodide indicated the location of nucleus. (B) Genomic DNA of Hep G2 cells was extracted and collected 24-h after PDE of verteporfin. Then a DNA gel electrophoresis was conducted. M denotes 100 base-pair DNA marker.

mitochondria play a major role in ROS-induced cell injury because they themselves are the primary intracellular ROS production sites [26–28], as well as the most susceptible target of ROS [29–32]. Glutathione (GSH) is the principal non-protein thiol and is present up to 10 mM in many cells and thus provides a primary defense against oxidative stress by its ability to scavenge free radicals or to participate in the reduction of H_2O_2 [33,34]. Furthermore, GSH, not synthesized in mitochondria, must be synthesized in the cytosol and subsequently transported into the mitochondria by a specific transporter [35]. It is known that the oxidized GSSG is not exported into the cytosol for its reduction to GSH [36]. Therefore, mitochondrial NADPH is necessary for the regeneration of GSH from GSSG catalysed via mitochondrial GSH reductase. Thus, the limited abundance of GSH in mitochondria couldmay play a pivotal role against ROS-induced oxidative stress. In this study, oOur data indicate that PDE of verteporfin was capable of depleting over 90% of GSH of HepG2 cells in 10 min. Since verteporfin has been proved to be a mitochondria-directed photosensitizer, we thus presume that the majority of GSH exhaustion should primarily occur in the mitochondria.

There are several pathways that can help to interpret the possible mechanism(s) associated with mGSH depletion in HepG2 cells afterinduced by PDE of verteporfin. First, although GSH is not synthesized in mitochondria, these organelles have the capacity to concentrate cellular level of GSH to a certain level, which might be exhausted if ROS/RNS was strikingly produced [37,38]. In this study, we show that the PDE of verteporfin could rapidly provoke the over-production of nitric oxide (NO), as reflected by the observation that the principal intensity of green fluorescence of oxidized DAF probe was concentrated in the perinuclear region consistent with the mitochondrial localization. Thus, the depletion of mitochondrial GSH can then proceed via the initial interaction of NO and GSH:

$$NO + GSH \Rightarrow GSNO^{\bullet} + H^{+} \quad (1)$$

Alternatively, H_2O_2 generated by the PDE of verteporfin can interact with ferrous (Fe^{2+}) or cuprous (Cu^{2+}) ions resulting in the formation of hydroxyl radicals ($^{\bullet}OH$) via the Fenton (reaction 2) or Harber-Weiss (reaction 3) reaction:

$$H_2O_2 + Fe^{2+} \text{ (or } Cu^{2+}) \Rightarrow {}^{\bullet}OH + OH^{-} + Fe^{3+} \quad (2)$$

$$O_2^{\bullet-} + H_2O_2 \overset{Fe3+}{\Rightarrow} {}^{\bullet}OH + OH^{-} + O_2 \quad (3)$$

Hydroxyl radicals thus formed are capable of abstracting a hydrogen atom from GSH with commensurate formation of a thiyl radical (GS·).

$$^{\bullet}OH + GSH \Rightarrow H_2O + GS^{\bullet} \quad (4)$$

The depletion of mGSH can then be effected via the termination reaction of a pair of GS· radicals to produce GSSG, an oxidized form of GSH.

$$GS^{\bullet} + GS^{\bullet} \Rightarrow GSSG \quad (5)$$

In addition, if membrane lipid peroxidation occurs, the formation of peroxyl radicals (ROO·) is an inevitable outcome. This radical species can also abstract a hydrogen atom from GSH with commensurate formation of thiyl radical. Thus, it is possible that mGSH can also be depleted via this pathway.

There are several possible deleterious effects that may be associated with the ROS/RNS-evoked mGSH depletion and lipid peroxidation instigated by the PDE of verteporfin. Our data presented here are consistent with the notion that GSH depletion can be an effective strategy to sensitize cancer cells to undergo apoptosis, as reported elsewhere in the literature [20,39–41]. Thus, it is also conceivable that if the membrane thiol group of essential cellular organelles were oxidized via ROS/RNS generated by the PDT of verteporfin, the functional consequence could be an alteration of cellular permeability. If this event occurs, cytosolic calcium (cCa^{2+}) can indiscriminately influx into mitochondria, resulting in mitochondrial Ca^{2+} overload. The notion that mCa^{2+} overload is associated with mROS formation and apoptosis has been reported elsewhere [42]. Indeed, deprivation of mitochondrial calcium using EGTA did reduce the production of ROS by a certain amount (data not shown). Furthermore, the production of mROS due to mitochondrial dysfunction whichthat could result from the mitochondrial membrane potential depolarization and ATP depletion has also been documented [4]. Consequently, we surmise that this self-perpetuating vicious cycle can play a role in the PDE of verteporfin-induced apoptosis of HepG2 cells in this study. Interestingly, when mitochondria uptake excessive Ca^{2+} (mM range or referred to as massive loading) due to the oxidative membrane damages, this can lead to a swelling phenomenon and an alteration of morphology that may consequently contribute to the initiation of apoptotic cell death. However, as indicated by the viability assays shown in Figure 6C, the toxic effect of PDE was not jeopardized by deprivation of mitochondrial calcium using EGTA.

In summary, we have also demonstrated unequivocally that depletion of glutathione, release of cytochrome *c* and activation of caspase activity together constitute a likely upstream cascade of events that underlie the final apoptotic death of HepG2 cells induced by PDE of verteporfin, as manifested by DNA ladder fragmentation and DNA breakage demonstrated by TUNEL assay. These results enable a connection between PDE of verteporfin and the ROS/RNS-mediated occurrence of apoptotic cell death in this cell model to be made.

We also re-confirm that in addition to a low dark toxicity, verteporfin is also a mitochondrially-directed agent by using Mitotracker Green to localize the target site. As a result of these advantages, verteporfin should be a versatile photosensitizer for future use in combination therapeutic regimens for preferential photo-killing of cancer cells. Importantly, we also found that the PDE of verteporfin could preferentially eradicate HepG2 cells, which have otherwise proved to be highly resistant to chemotherapy and radiotherapy. This observation could serve as a basis for widening its applicability to deal with more types of cancer cells.

Acknowledgement

The technical assistance of Ms Chyi-yun Hwung is deeply appreciated. Also, we thank Dr Michael Byford for his helpful comments on cleaning up the writing for this manuscript.

Declaration of interest: The authors report no conflicts of interest. The authors alone are responsible for the content and writing of the paper.

References

[1] Levy JG. Photosensitizers in photodymanic therapy. Semin Oncol 1994;2:4–10.
[2] Yang J, Liu K, Bhalla K, Kim CN, Ibrabo AM, Cai J, Peng TI, Jones DP, Wang X. Prevention of apoptosis by Bcl-2: release of cytochrome c form mitochondria blocked. Science 1997;275:1129–1132.
[3] Read JC. Cytochorme c: can't live with it – can't live without it. Cell 1997;91:559–562.
[4] Jou MJ, Jou SB, Chen HM, Lin CH, Peng TI. Critical role of mitochondrial reactive oxygen species formation in visible laser irradiation-induced apoptosis in rat brain astrocytes (RBA-1). J Biomed Sci 2002;9:507–516.
[5] Szewczyk A, Klojtczak L. Mitochondria as a pharmacological target. Pharmacol Rev 2002;54:101–127.
[6] Modica J, Singh K. Mitochondria as target for detection and treatment of cancer. Expert Rev Mol Med 2002;4:1–19.
[7] Decandin D, Marzo I, Brenner C, Kroemer G. Mitochondria in chemotherapy-induced apoptosis: a prospective novel target of caner therapy. Int J Oncol 1998;12:141–152.
[8] Peng TI, Chang CJ, Guo MJ, Wang YH, Yu JS, Wu HY, Jou MJ. Mitochondria-targeted photosensitizer enhances the photodynamic effect-induced mitochondrial dysfunction and apoptosis. Ann NY Acad Sci 2005;1042:419–428.
[9] Richter AM, Jain AK, Canaan AJ. Photosensitizing efficiency of two regioisomers of the benzoporphyrin derivative monoacid ring A (BPD-MA). Biochem Pharmacol 1992;43:2349–2358.
[10] Panjehpour M, Denovo RC, Petersen MG. Photodynamic therapy using Verteporfin (Benzoporphyrin derivative monoacid ring A, BPD-MA) and 630 nm laser light in canine esophagus. Lasers Surg Med 2002;30:26–30.
[11] Gilaberte Y, Pereboom D, Carapeto FJ, Alda JO. Flow cytometry study of the role of superoxide anion and hydrogen peroxide in cellular photodestruction with 5-amionlevulinic acid-induced protoporphyrin IX. Photodermatol Photoimmunol Photomed 1997;13:43–49.
[12] Hadjur C, Wagnieres G, Ihringer F, Monnier P, van der Bergh H. Production of the free radicals $O2^{\bullet-}$ (and $^{\bullet}OH$ by irradiation of the photosensitizer zinc (II) phthalocyanine. J Photochem Photobiol B 1997;38:196–202.
[13] Friedmann H, Lubart R, Laulicht I, Rochkind S. A possible explanation of laser-induced stimulation and damage of cell culture. J Photochem Photobiol B 1991;11:87–91.
[14] Luo Y, Chang CK, Kessel D. Rapid initiation of apoptosis by photodynamic therapy. Photochem Photobiol 1996;63: 528–534.
[15] Oleinick NL, Evans HH. The photobiology of photodynamic therapy: cellular targets and mechanisms. Radiat Res 1998; 150:s146–s156.
[16] Lam M, Oleinick NL, Nieminen AL. Photodynamic therapy-induced apoptosis in epidermoid carcinoma cells. Reactive oxygen species and mitochondrial inner membrane permeabilization. J Biol Chem 2001;276:47379–47386.
[17] Lebel CP, Ischiropoulos H, Bondy SC. Evalution of the probe 2', 7'-dichlorofluorescein as an indicator of reactive oxygen species formation and oxidative stress. Chem Res Toxicol 1992;5:227–231.
[18] Carter WO, Narayanan PK, Robinson JP. Intracellular hydrogen peroxide and superoxide anion detection in endothelial cells. J Leuko Biol 1994;55:253–258.
[19] Ball BA, Vo A. Detection of lipid peroxidation in equine spermatozoa based upon the lipophilic fluorescent dye C_{11}-BODIPY$^{581/591}$. J Andro 2002;23:259–269.
[20] Chen CH, Liu TZ, Chen CH, Wong CH, Chen CH, Lu FJ, Chen SC. The efficacy of protective effects of tannic acid, gallic acid, ellagic acid, and propyl gallate against hydrogen peroxide-induced oxidative stress and DNA damages in IMR-90 cells. Mol Nutr Food Res 2007;51:962–968.
[21] Clernent MV, Pervaiz S. Intracellular superoxide and hydrogen peroxide concentrations: a critical balance that determined survival or death. Redox Rep 2001;6:211–214.
[22] Ali SM, Chee SK, Yuen GY, Olivo M. Hypocrellins and hypericin induced apoptosis in human tumor cells: a possible role of hydrogen peroxide. Int J Mol Med 2002;9:461–472.
[23] Gupta S, Ahmad N, Mukhtar H. Involvement of nitric oxide during phthalocyanine (Pc4) photodynamic therapy-mediated apoptosis. Cancer Res 1998;58:1785–1788.
[24] Lu Z, Tao Y, Zhou Z, Zhang J, Li C, Ou L, Zhao B. Mitochondrial reactive oxygen species and nitric oxide-mediated cancer cell apoptosis in 2-butylaino-2-demeththoxyhypocrellin B photodynamic treatment. Free Radic Biol Med 2006;41: 1590–1605.
[25] Huang Z, Xu H, Meyers AD, Musani AI, Wang L, Tagg R, Barqawi AB, Chen YK. Photodynamic therapy for treatment of solid tumors-potential and technical challenges. Technol Cancer Res Treat 2008;7:309–320.
[26] Boveris A, Chance B. The mitochondrial generation of hydrogen peroxide: generation properties and effect of hyperbaric oxygen. Biochem J 1973;134:707–716.
[27] Cai J, Jones DP. Superoxide in apoptosis: mitochondrial generation triggered by cytochrome c loss. J Biol Chem 1998;273:11401–11404.
[28] Turrens JF. Superoxide production by the mitochondrial respiratory chain. Biosci Rep 1997;17:3–8.
[29] Atlante A, Calissano P, Bobba A, Azzariti A, Marra E, Passarella S. Cytochrome c is released from mitochondria in a reactive oxygen species (ROS)-dependent fashion and can operate as a ROS scavenger and as a respiratory substrate in cerebellar neuron undergoing excitotoxic death. J Biol Chem 2000;275:37159–37166.
[30] Backway KL, McCullech EA, Chow S, Hedley DW. Relationship between the mitochondrial permeability transition and oxidative stress during ara-c toxicity. Cancer Res 1997;57:2446–2451.
[31] Kowaltowshi AJ, Vercesi AE. Mitochondrial damage induced by condition of oxidative stress. Free Radic Biol Med 1999; 26:463–471.
[32] Liu SS. Generating, portioning, targeting and functioning of superoxide in mitochondria. Biosci Rep 1997;17:259–272.

[33] Wefers H, Sies H. Oxidation of glutathione by the superoxide radical to the disulfide and the sulfonate yielding singlet oxygen. Eur J Biochem 1983;137:29–36.
[34] Winterbourn CC, Metodiewe D. The reaction of superoxide with reduced glutathione. Arch Biochem Biophys 1994;314: 284–290.
[35] Garcia-Ruiz C, Morales A, Colell A, Rodes J, Yi JR, Kaplowitz N, Fernondez-Checa JC. Evidence that the rat hepatic mitochondrial carrier is distinct from the sinusoidal and canalicular transporter for reduced glutathione. Expression studies in Xenopus loevis oocytes. J Biol Chem 1995;270:1596–15949.
[36] Olafsdottir K, Reed DJ. Retention of oxidized glutathione by isolated rat liver mitochondria during hydroperoxide treatment. Biochim Biophys Acta 1988;964:377–382.
[37] Fernandez-Checa JC, Kaplowitz N. Hepatic mitochondrial glutathione: transport and role in disease and toxicity. Toxocal Appl Pharmacol 2005;204:263–273.

This paper was first published online on Early Online on 29 October 2009

[38] Soderdahl T, Enoksson M, Lundberg M, Holmgren A, Ottersen OP, Orrenius S, Blocsfold G, Cotgreave IA. Visualization of the compartmentalization of glutathione and protein-glutathione mixed disulfide in cultures cells. FASEB J 2003;17:124–126.
[39] Fukumura D, Kashiwagi S, Jain RK. The role of nitric oxide in tumor progression. Nat Rev Cancer 2006;6:521–534.
[40] Kachadourian R, Day BJ. Flavonoid-induced glutathione depletion: potential applications for cancer treatment. Free Radic Biol Med 2006;41:65–76.
[41] Trachootham D, Zhou Y, Zhang H, Demizu Y, Chen Z, Pelicano H, Chiao PJ, Achanta G, Arlinghaus RB, Liu J, Huang P. Selective killing of oncogenically transformed cells through a ROS-mediated mechanism by β-phenylethyl isothiocyanate. Cancer Cell 2006;10:241–252.
[42] Chakraborti T, Das S, Mondal M, Roychoudhury S, Chakraborti S. Oxidant, mitochondria and calcium: an overview. Cell Signal 1999;11:77–85.